Low-temperature anomalies of the dielectric permeability of $Sn_2P_2S_6$ crystals FREE

H. Ban ✉ ⓘ ; D. Gal ⓘ ; A. Kohutych ⓘ ; A. Molnar ⓘ

Check for updates

View Online   Export Citation   CrossMark

Low-temperature anomalies of the dielectric permeability of $Sn_2P_2S_6$ crystals

View Online   Export Citation   CrossMark

H. Ban,[1,a] D. Gal,[1,2,b] A. Kohutych,[1,c] and A. Molnar[1,d]

AFFILIATIONS

[1]Department of the Physics of Semiconductors, Uzhhorod National University, Uzhhorod 88000, Ukraine
[2]WIGNER Research Center for Physics, P. O. Box 49, Budapest H-1525, Hungary

[a]banhenrietta@gmail.hu
[b]galdavidagu7@gmail.com
[c]a.kohutych@gmail.com
[d]**Author to whom correspondence should be addressed:** alex.molnar@uzhnu.edu.ua

ABSTRACT

Low-temperature anomalies of dielectric permittivity of $Sn_2P_2S_6$ crystals were investigated. It is shown that these phenomena have a relaxation character and the observed anomalies could be related to the small hole polarons dynamics with donor-acceptor compensation processes in lattice with tin and sulfur vacancies. To confirm it, we measured the dielectric properties of tin-enriched and sulfur-enriched crystals. It is shown that deviation from stoichiometry leads to a significant change in the low-temperature anomalies of dielectric losses.

Published under an exclusive license by AIP Publishing. https://doi.org/10.1063/10.0023893

1. INTRODUCTION

$Sn_2P_2S_6$ crystals are uniaxial ferroelectric semiconductors with a second-order phase transition (PT) from the paraelectric phase ($P21/n$) to the ferroelectric phase (Pn) at a temperature of $T_0 \approx 337$ K and a bandgap width ≈ 2.5 eV.[1] Due to its unique properties, it is of great interest in terms of practical use as a pyroelectric transducer,[2] piezoelectric sensor,[3] memory cell with the ability to store several bits of information,[4] as multifunctional alternative power supplies,[5] nonlinear optical elements,[6] etc. It is possible to extend its operating temperature range (raising the phase transition temperature up to 360 K) by doping with germanium.[7] However, the main difficulty for the implementation of $Sn_2P_2S_6$ crystals in real production is the relatively low reproducibility of its physical parameters. To date, two methods of synthesis and growth of single crystals of $Sn_2P_2S_6$ are known: the Bridgman–Stockbarger (BR) method of directed crystallization from the melt[8] and obtaining it from the gas phase by chemical transport reactions (CTR).[9] Both methods make it possible to obtain crystals of large size (diameter up to 3 cm and length up to 5 cm). Samples obtained by these two methods with the same chemical composition have significantly different physical properties. Crystals grown by the Bridgman method are relatively opaque (although it is possible to obtain more or less transparent samples), have low dielectric losses (10^{-3}), and record values of dielectric constant (10^5 at phase transition), bulk piezoelectric and pyroelectric coefficients. They are more suitable for electrophysical applications. In turn, crystals obtained by chemical transport reactions have excellent optical properties (transparent). But in comparison with BR samples, their electrophysical properties are much worse—they have losses at the level of 10^{-1}–10^{-2}, higher conductivity, and lower value of dielectric constant (10^3–10^4 at the phase transition). Due to the higher electrical conductivity and the screening phenomena associated with it (caused by near-electrode volumetric charges), pyroelectric and piezoelectric indices are also underestimated. The method of preparation also significantly affects the physical phenomena occurring in these samples. In BR crystals a relaxation change in the phase transition character is observed,[10] while in CTR samples this phenomenon is absent. The behavior of $Sn_2P_2S_6$ crystals also differs significantly in the region of low temperatures (below 0°C).[11]

Previous studies have examined how production methods affect the low-temperature properties of crystals. In 1998, the low-temperature dielectric dispersion in $Sn_2P_2S_6$ crystals was initially documented.[12] The authors noted poor repeatability of the results at 220 K, and the anomaly at 60 K was explained by structural disorder with polar symmetry (dipole glass state). Later, the paper[13]

presents the thermoluminescence results of $Sn_2P_2S_6$ crystals. It is shown that in the temperature range 15–240 K 17 thermoluminescence lines are observed, most likely caused by the corresponding shallow traps of charge carriers with an activation energy of 0.05–0.5 eV. In addition, noticeable differences were observed in the spectra of crystals grown by various methods. The same authors conducted studies on the photoluminescence spectra of $Sn_2P_2S_6$ and discovered emission peaks in the red and near-infrared regions at low temperatures.[14,15]

It is logical to assume that the behavior of physical properties in $Sn_2P_2S_6$ crystals' ferroelectric phase depends on the domain structure. Similar studies were carried out in Ref. [16], though only for samples grown by the method of gas transport reactions with high conductivity. The authors conclude that the dielectric anomaly has a relaxation character and is due mainly to the nonlinear component in the dielectric response of domain walls and is a consequence of a sharp increase in the anharmonicity of the crystal lattice.

We previously examined how the preparation method affects the dielectric properties and Raman scattering spectra of $Sn_2P_2S_6$ crystals.[17] It was hypothesized that the observed low-temperature dielectric anomalies of these crystals are related to the dynamics of polarons due to donor-acceptor compensation. The position of shallow acceptor states due to tin vacancies and deep donor levels bound by sulfur vacancies correlate with the activation energies of dielectric relaxation processes. Nevertheless, we lacked conclusive experimental evidence, prompting us to conduct further research.

In this paper, we present the results of our study on how deviations from stoichiometry affect the low-temperature behavior of $Sn_2P_2S_6$ samples.

2. CRYSTAL GROWING

The growth of single crystals was carried out by the method of directed crystallization from the melt (Bridgman–Stockbarger method)[18] in two-zone furnaces. Temperature control and regulation were carried out by the temperature controller RIF-101 with an accuracy of ±1 K. The crystals were grown at a hot zone temperature of 1100 K and a cold zone temperature of 870 K. The temperature gradient in the crystallization zone was 3–4 K/mm, the growth rate was 1.5 mm/day, and the cooling rate was 150 K/day. As a result, single crystals of the following compositions were obtained: $Sn_2P_2S_6$, $Sn_{1.95}P_2S_{6.05}$, and $Sn_{2.05}P_2S_{5.95}$ of yellow-orange to light brown color. The color of the single crystals depended on the tin content (more Sn—darker crystals). Samples of $Sn_2P_2S_6$, obtained from the gas phase and without any deviation from stoichiometry, were also utilized for comparison.

Energy-dispersive spectroscopy (EDS) was applied for the evaluation of the chemical composition of the samples using a TESCAN MIRA 3 Scanning Electron Microscope equipped with a Thermo Scientific EDS system in the WIGNER Research Center for Physics. The obtained EDS compositions were as follows: $Sn_2P_2S_6$ (Bridgeman sample), $Sn_2P_2S_6$ (gas transport sample, within the accuracy of the methodology), $Sn_{1.95}P_2S_{6.05}$ and $Sn_{2.05}P_2S_{5.95}$.

3. EXPERIMENTAL EQUIPMENT

Measurements of temperature dependences were carried out using an automated computer-controlled system[19] in an immersion-type cryostat[20] based on Measurement Computing USB-TEMP-AI data acquisition device and Linear Programmable DC Power Supply OWON ODP3033, which allows us to change the heating and cooling rate in the range from 0.001 to 1 K/min. As a temperature sensor, the PT100/1509A platinum thermistor of TDI Ltd. company (England) was applied. The temperature measurement resolution was 0.001 K with an absolute accuracy of ±2.9 K at 73 K and 0.27 K at 373 K.

To measure the dielectric constant, an LCR GW Instek LCR-819 meter with a frequency range of 12 Hz–100 kHz and a measuring voltage of 50 mV–1.25 V was chosen. To perform experiments under the same conditions, the measuring voltage on the samples was varied according to their thickness. Taking into account that the coercive field of $Sn_2P_2S_6$ crystals is 700 V/cm[1], our measurements were carried out in the region of linearity of the dielectric response.

To measure the dielectric hysteresis loops, a standard Soer-Tauer circuit[21] was used, with a reference high-voltage low-loss 2.2 μF Teflon capacitor (K73-17). The high-voltage amplifier to generate the excitation voltage was based on a Burr-Brown (Texas Instruments) 3584 high-voltage operational amplifier. We used an EMCO E03CTR (1QBEJ AH) DC-DC voltage converter from 12 to ±150 V as the power supply. The excitation signal was generated by the software and fed from the output of the National Instruments USB6211 module, and its two ADC inputs were used to read the voltage of the X and Y channels. The control program was written in the LabVIEW environment.

4. EXPERIMENTAL RESULTS

Plates of polar [100] cut samples, ranging from 5×5 to 8×8 mm with a thickness of 2–3 mm, were used for the experiment. Silver paste electrodes were applied on the largest (001) faces, which was nearly normal to the spontaneous polarization direction.

The temperature change rate for all experiments was 0.1 K per minute. It is prohibited to change the cooling or heating rate during the measurement of electrophysical parameters of crystals as it results in "false anomalies" of studied parameters like dielectric permittivity and conductivity. Because the investigated $Sn_2P_2S_6$ crystals are ferroelectric semiconductors, the sample background has a significant influence on the obtained experimental data. This results in a "memory" of certain factors, such as illumination, cooling rate, electric field, etc., which affect the size of domains in the ferroelectric phase, dynamics of the population of sticking levels in the band gap, and shielding by near-electrode charges. This leads to certain difficulties in comparing data obtained in different experiments. Before the measurements, each $Sn_2P_2S_6$ crystal was pre-annealed at 380 K for 3 h to remove any preexisting history. Based on our previous studies, this process can effectively eliminate the prehistory of the samples and standardize them for equal experimental conditions.

4.1. Gas phase and bridgeman samples

We used $Sn_2P_2S_6$ crystals grown from the gas phase as a "reference sample". These samples have similar dielectric properties to crystals with stoichiometry deviation and annealed in different atmospheres. The components of the complex dielectric permittivity

$\varepsilon^* = \varepsilon' - j\varepsilon''$ have approximately the same order of magnitude (ε' at the phase transition ≈ 3000, $\varepsilon'' \approx 300$ and, accordingly, tg $\delta \approx 0.1$), including the dissipation factor tg $\delta = \varepsilon''/\varepsilon'$, which is measured by the applied equipment. Later, it will be shown that crystals grown by the Bridgman method from the melt have significantly different electrophysical parameters than those previously listed.

For all studied samples in this paper, we will provide both the temperature dependences of the components of the complex dielectric permittivity and the dissipation factor. This is because the strong temperature dependence of the dielectric permittivity leads to a change in the ratio of anomalies in the range of 120–270 K, especially when approaching the phase transition temperature. Figures 1(d) and 2(d) show that the dielectric loss tangent is twice as high in the region we studied compared to gas-transport samples at phase transition, and almost identical for the crystals grown from melt.

As we can see in Fig. 1, at the temperature of the second-order phase transition $T_c \approx 337$ K at the dependences of $\varepsilon'(T)$, $\varepsilon''(T)$, and $\varepsilon''/\varepsilon'(T)$ there is a strong anomaly, which in the case of $\varepsilon'(T)$ reaches a record value of $1.1 \cdot 10^5$. In the temperature dependence of dielectric losses, two anomalies are observed at temperatures of 190 and 260 K in the 160–280 K region [inset in Fig. 1(b)]. This is also well seen in the $\varepsilon''/\varepsilon'(T)$ plot of Fig. 1(d). These anomalies are characterized by strong amplitude hysteresis.
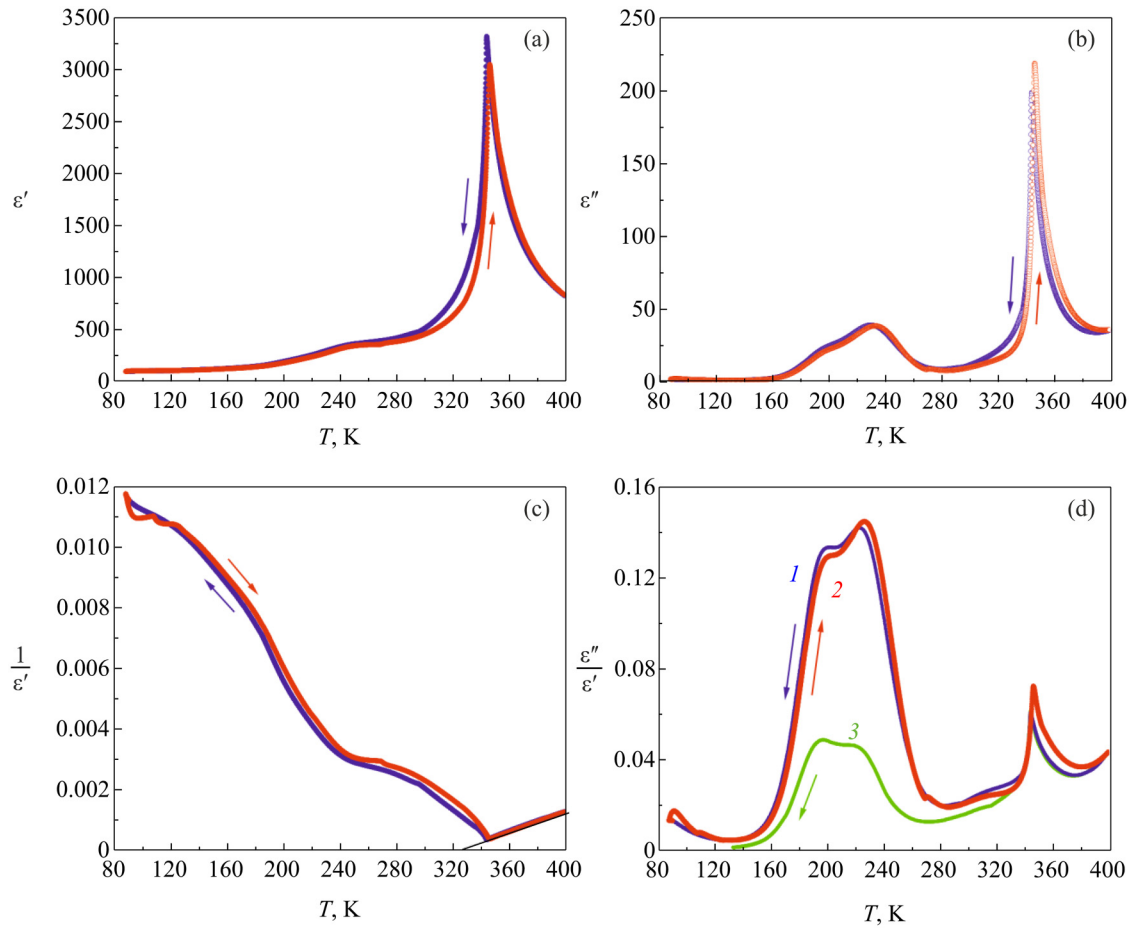
The temperature dependence of the inverse value of the dielectric permittivity follows the Curie–Weiss (CW) law in both the paraelectric ($T > T_c$) and ferroelectric ($T < T_c$) phases up to 160 K. Below this temperature, a deviation from the CW law is observed.

Figure 2 shows similar plots for the crystal obtained from the gas phase. They are noticeably different from the ones described above. The phase transition anomaly is more smeared [Figs. 2(a) and 2(b)], the maximum value of $\varepsilon'(T)$ is 30 times smaller than in the case of the Bridgman sample and reaches a value of 3400, and is characterized by a large hysteresis. The low-temperature anomalies here are concentrated in a narrower range of 160–260 K and have
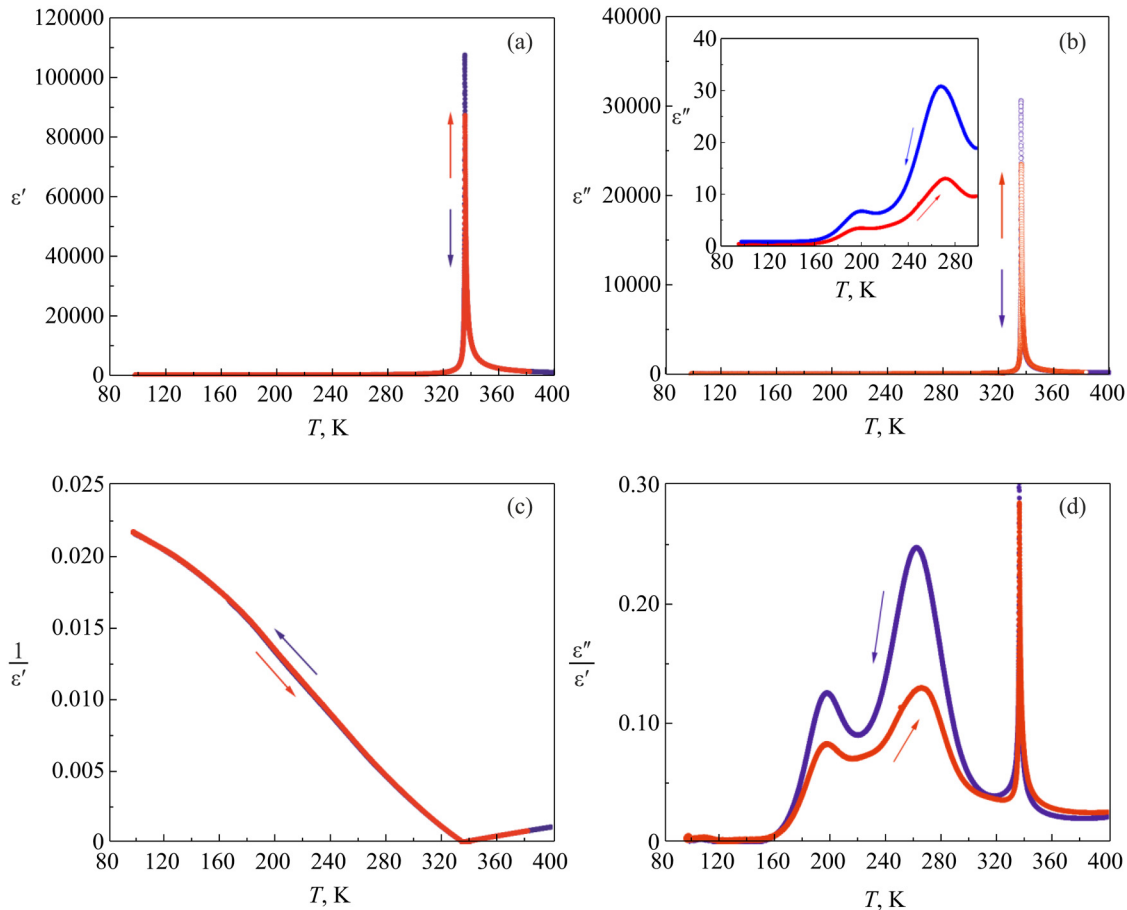
FIG. 1. Temperature dependences at cooling and heating of dielectric permittivity (a), dielectric loss (b), the inverse value of the dielectric permittivity (c), and dissipation angle tangent (d) of $Sn_2P_2S_6$ crystal grown from melt by Bridgman method measured at 10 kHz.

FIG. 2. Temperature dependences at cooling and heating of dielectric permittivity (a), dielectric loss (b), the inverse value of the dielectric permittivity (c), and dissipation factor (d) of $Sn_2P_2S_6$ crystal grown from the gas phase by chemical transport reactions measured at 10 kHz. Line 3 in graph (d) shows the effect of illumination with white light.

practically no hysteresis in amplitude, as in the case of the BR samples. On the temperature dependence of $\varepsilon'(T)$ we observe a distinct bend at 240 K. The temperature dependence of $1/\varepsilon'(T)$ is also more complicated [Fig. 2(c)]. In the paraelectric phase $(T > T_c)$, the Curie–Weiss law is not poorly satisfied (although at increasing scale there is a deviation from the CW law with increasing temperature, which is characteristic of this type of crystals and is due to their greater conductivity, and accordingly its thermal activation). In the ferroelectric phase $(T < T_c)$, we see a strong deviation from the Curie–Weiss law both at 240 K and in the region of lower temperatures < 140 K.

4.2. Stoichiometry deviation

Earlier[17] we showed that low-temperature anomalies of dielectric permittivity in the region of 160–280 K, most likely due to the formation and annihilation of small hole and electron polarons

involving acceptor levels, associated with tin vacancies and donor centers caused by sulfur vacancies in gap energy states of $Sn_2P_2S_6$ crystals. The above anomalies are difficult to detect and interpret due to the blurred maximum associated with domain structure freezing. It is complicated to observe these anomalies, because the dielectric permittivity continuously increases as the temperature approaches the phase transition. There was no direct evidence that tin or sulfur vacancies caused the observed anomalies. In this study, we obtained[18] and analyzed samples with sulfur excess (and tin deficiency) and tin excess (and sulfur deficiency). Figure 3 displays the measurements' outcomes.

$Sn_{1.95}P_2S_{6.05}$ crystals with excess sulfur content have 10 times lower dielectric constant at phase transition compared to pure gas-phase $Sn_2P_2S_6$ [Fig. 3(a), curve 3]. In this case, as can be seen in Fig. 3(b), the dielectric losses on the PT also decrease. This can be explained by the "trapping" of free charge carriers by acceptor levels caused by tin vacancies. This is confirmed by the disappearance of
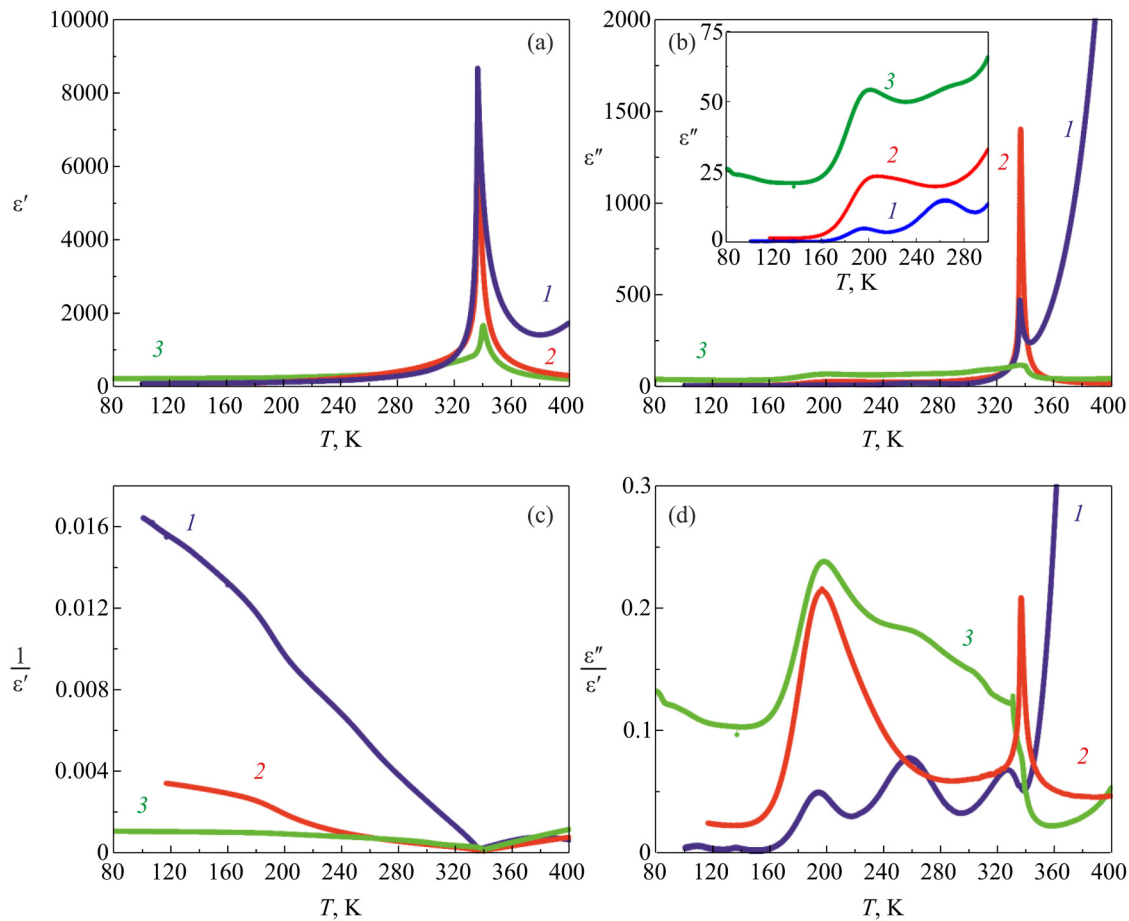
FIG. 3. Temperature dependences of dielectric permittivity (a), dielectric loss (b), the inverse value of the dielectric permittivity (c), and dissipation factor (d) of $Sn_2P_2S_6$ crystal grown from the gas phase (*1*), $Sn_{2.05}P_2S_{5.95}$ (*2*), $Sn_{1.95}P_2S_{6.05}$ measured at 1 kHz (*3*).

the high-temperature "tail" $\varepsilon''(T)$ in the interval 340–400 K, which, as noted earlier, is associated with the growth of the conductivity of the sample. At temperatures below the phase transition, losses increase. This is noticeable in the 160–280 K range we investigated. As can be seen in the inset of Fig. 3(b), the anomaly at temperature ≈ 200 K increases strongly, while the peak at 260 K practically disappears (or is very strongly blurred). This can be seen especially well in the temperature dependence of the dielectric loss angle tangent [Fig. 3(d), curve *3*], which is not so sensitive to the "background processes" listed earlier. On the temperature dependence of the inverse value of dielectric permittivity in the ferroelectric phase [Fig. 3(c)], we see a deviation from the Curie–Weiss law at a temperature of 200 K for all compositions. In the paraelectric phase, a strong deviation from the Curie–Weiss law due to conductivity is observed.

The deviation of stoichiometry in the direction of increasing tin and decreasing sulfur content in the samples $Sn_{2.05}P_2S_{5.95}$ also leads to a decrease in the maximum dielectric constant at the phase

transition [approximately 1.5 times, compared to curve *1*, Fig. 3(a)], which in both cases may be associated with an increase in the defectivity of the structure, which in turn reduces the mobility of dipoles in the external measuring field. In this case, tin vacancies show much stronger behavior than sulfur vacancies. Compared to the stoichiometric $Sn_2P_2S_6$ sample, the dielectric losses increase significantly by 3–4 times both at PT and in the low-temperature region. Additionally, the sharp increase in $\varepsilon''(T)$ disappears in the 340–400 K interval. As can be seen in Fig. 3(d), curve *2* [and also in the inset of Fig. 3(b)], there is an increase in the anomaly at 200 K in the 160–280 K region compared to curve *1*, and a complete absence of the peak at 260 K.

4.3. Post-growth processing

As previously demonstrated,[22] an effective method to change the chemical composition of $Sn_2P_2S_6$ single crystals is through post-growth treatment. Post-growth annealing of single crystals in a

vacuum and a sulfur atmosphere were used to modify the chemical composition. For this purpose, a sample obtained from the gas phase in the form of a $5 \times 5 \times 1.2$ mm plate was placed in an evacuated quartz ampoule (3 Pa) with a wound nichrome heater. The ampoule was heated to a temperature of 523 K and incubated for 144 h. In the case of annealing in a sulfur atmosphere, the sulfur powder was also added to the evacuated ampoule and vaporized during heating, creating a sulfur atmosphere in the ampoule. The ampoule was heated to a temperature of 548 K and held for 36 h. After annealing, slow cooling, and sample extraction, the surface of the samples was sanded to obtain 1 mm thick samples. Crystals annealed in a sulfur atmosphere became lighter, while those annealed in a vacuum became darker.

It is logical to assume that the annealing of $Sn_2P_2S_6$ crystals in a sulfur atmosphere will lead to their "enrichment" with sulfur. Although $Sn_2P_2S_6$ is a 3D crystal, it has cleavage planes in which a rather efficient intercalation process is observed.[23] Accordingly, sulfur atoms at high temperatures can penetrate quite deeply into

the sample, causing its "oversaturation" with sulfur. We obtain samples with increased sulfur content.

Vacuum annealing has the opposite effect. When heating $Sn_2P_2S_6$ crystals in a pumped-out ampoule, a change in color of the inner surface of the ampoule is observed (when opening the ampoule after cooling, a characteristic smell of sulfur is felt), the loss of mass of the sample, which can most likely be explained by the evaporation of sulfur during heating of the sample. We obtain samples with decreased sulfur content.

Of course, this post-growth treatment does not allow for a uniform distribution of excess or deficiency of sulfur. This phenomenon will be more pronounced in the near-surface regions. But we have also investigated similarly treated crystals since post-processing makes it much easier to create samples with deviations in sulfur content than to grow them.

As we can see in Fig. 4, annealed crystals also strongly change their electrophysical properties. Annealing both in the sulfur atmosphere and in vacuum leads to an increase in dielectric constant
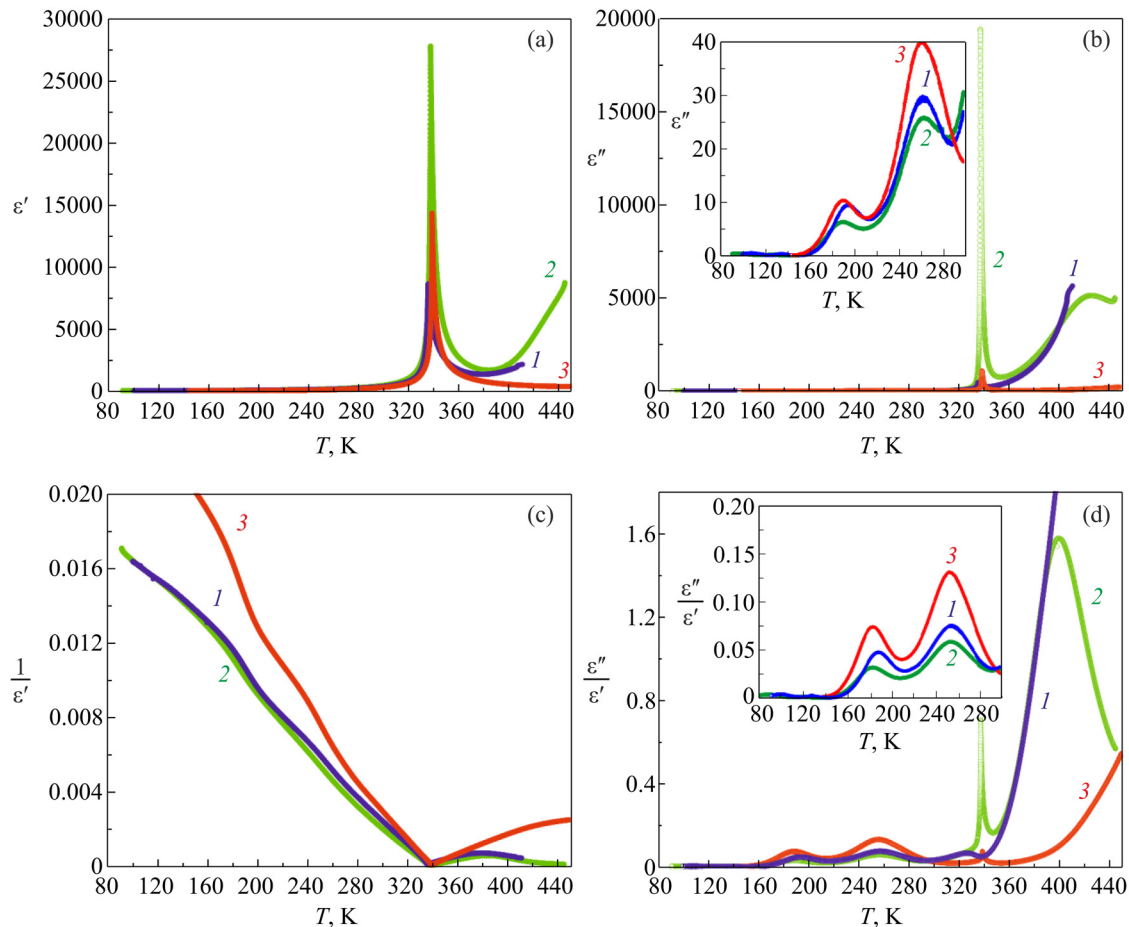
FIG. 4. Temperature dependences of dielectric permittivity (a), dielectric loss (b), the inverse value of the dielectric permittivity (c), and dissipation factor (d) of $Sn_2P_2S_6$ crystal grown from the gas phase (*1*), annealed in the sulfur atmosphere (*2*), vacuum annealed measured at 1 kHz (*3*).

over the entire temperature range, with annealing in the sulfur atmosphere giving a more appreciable increase [by a factor of 4 on the PT compared to curve *1*, and also noticeably on the inverse value of dielectric constant, Fig. 4(c)] than annealing in vacuum [by a factor of 2 on the PT, Fig. 4(a), curve *3*]. Dielectric losses are even more sensitive to post-treatment. Annealing in vacuum leads to a 3-fold increase in dielectric losses on the PT [Fig. 4(b), curve *3*], while the amplitude of the anomalies at 200 and 260 K also increases, which is visible in the insets of Figs. 4(b) and 4(d). And annealing in the sulfur atmosphere acts on the contrary, leads to a decrease in the anomalies at 200 and 260 K, and also strongly increases the PT losses [by 30 times compared to the reference crystal $Sn_2P_2S_6$, Fig. 4(b), curve *1*].

In graphs of Figs 4(b) and 4(d) we can notice maxima at temperature 400 K. This maximum sometimes occurs in pure, freshly grown $Sn_2P_2S_6$ crystals obtained by chemical transport reactions (almost never in Bridgman samples). This maximum can be explained as follows. As shown in Ref. 24, the main charge carriers in $Sn_2P_2S_6$ crystals in both paraelectric and ferroelectric phases are holes. With increasing temperature, the concentration of both the main charge carriers and thermally activated electrons, which compensate for each other, increases. However, the growth rate of electrons is greater than that of holes, and the intersection of these two processes just falls at this temperature. In pure CTR crystals, this occurs at a temperature of ≈ 450 K,[24] and annealing in a sulfur atmosphere leads to an increase in the concentration of electrons, which leads to a decrease in the temperature of the transition point from hole to electronic conduction.

This fact can be used to confirm that the ratio of charge carriers of different polarities has a significant effect on the low-temperature anomalies observed experimentally. From the above, we can conclude that stoichiometry deviation in sulfur and post-treatment in the sulfur atmosphere act differently.

Most likely, annealing leads to a change in chemical composition closer to the surface (or at a low depth), and promotes the formation at electrode volume charges, which have an "integral" effect on the studied samples, and do not affect the concentration of donor and acceptor levels in the bandgap.

4.4. Dielectric hysteresis loop

To reveal at electrode volume charge, we have investigated the switching processes of the described samples. The dielectric hysteresis loops of $Sn_2P_2S_6$ crystals annealed under different conditions are shown in Fig. 5. They show that the formation of near-electrode bulk charges manifests itself as an increase in the coercive field from 700 V/cm to 800–1000 V/cm, Figs. 5(b) and 5(c), the formation of a shifting internal field of 200 V/cm, which manifests itself in the displacement of the hysteresis loop, Fig. 5(c), and screening of spontaneous polarization, i.e., a decrease in its value from 13 to 8 $\mu C/cm^2$ for annealed samples.

In the case of $Sn_{2.05}P_2S_{5.95}$ and $Sn_{1.95}P_2S_{6.05}$ crystals, the dielectric hysteresis loops did not show the above changes. In addition to reducing the spontaneous polarization of annealed crystals, post-processing can be very useful for optimizing the switching processes in $Sn_2P_2S_6$ crystals in their practical applications, such as the creation of memory cells based on them Ref. 4.

4.5. Domain structure

As mentioned before, the investigated low-temperature anomalies are rather hard to detect from their coincidence with the anomaly due to the freezing of the domain structure.[11] Earlier work[16] even suggested that the observed dielectric permittivity anomaly is mainly due to the nonlinear component in the dielectric response of domain walls. This conclusion was made based on the strong dependence of the investigated anomaly on the measurement field strength. We carried out all measurements at a measuring field strength of 0.1 V/cm, which is 7000 times less than the coercive field of $Sn_2P_2S_6$ crystals, so we can safely say that we worked in the area of linearity of the dielectric response. Moreover, before carrying out the studies, the dielectric hysteresis loop was taken for each sample to confirm the absence of internal shifting electric fields. To verify and reject the assumption of domain causality of the investigated phenomena, we also carried out studies on monodomain and polydomain samples. The results of these measurements are presented in Fig. 6.

Curve *1* in Fig. 6(a) was obtained in the cooling mode at a rate of 0.1 K/min after the polydomain sample had been held at room temperature for 8 h. This was done to allow the domain structure to become sufficiently enlarged so that it could fix itself on the defects of the sample. With the "domain" nature of the phenomena under study, this should have manifested itself in a significant decrease in the anomalies at temperatures of 180 and 240 K, but in the experiment, we observe just the opposite behavior.
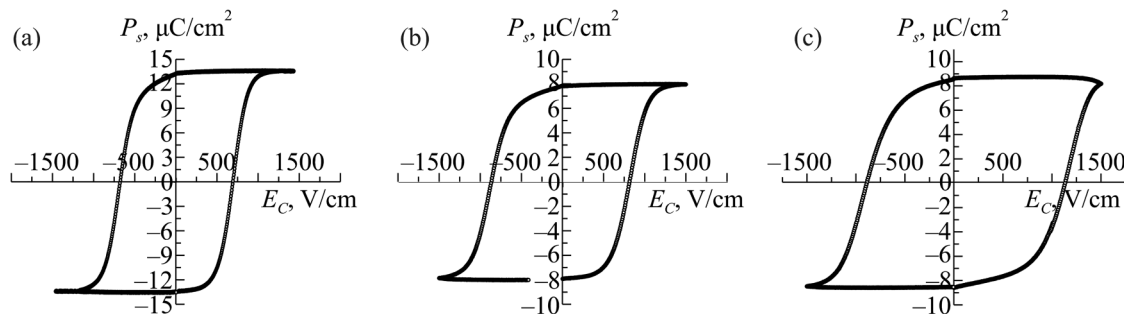

FIG. 5. Dielectric hysteresis loops obtained at 10 Hz for samples: pure $Sn_2P_2S_6$ (a), $Sn_2P_2S_6$ annealed in vacuum (b), $Sn_2P_2S_6$ annealed in the sulfur atmosphere (c).
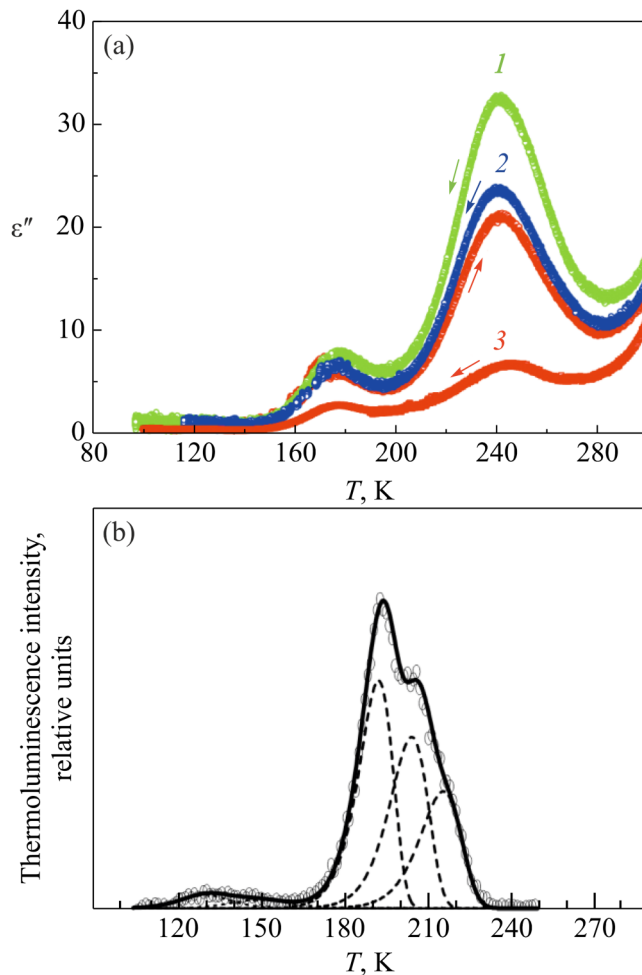
FIG. 6. Low-temperature section of the temperature dependences of dielectric losses (a) measured on the polydomain sample after temperature stabilization at 300 K for 8 h (*1*), in heating and cooling mode (*2*) at a rate of temperature change of 0.1 K/min, and on the monodomain sample (*3*). (b) Thermoluminescence curve[13] measured for the gas-transport crystal.

Curves *2* in Fig. 6(a) are obtained in the conventional regime of continuous cooling from 400 to 100 K, and reverse heating at a rate of 0.1 K/min. Since the domain structure at continuous temperature change does not have time to stabilize (enlarge, consolidate, and shield by free carriers), the dielectric response due to the dynamics of domain walls in the measuring field should be large compared to curve *1*. In the experiment, the opposite is true.

Monodomainization of the crystal was carried out by applying a high voltage (3000 V/cm, which is more than 4 times the coercive field) at a temperature of 400 K, followed by cooling of the sample under the field at a rate of temperature change of 0.1 K/min. After passing the phase transition and reaching room temperature, the high voltage was switched off and the sample was short-circuited, so that the bulk charge accumulated on the electrodes and in the

near-electrode regions could flow away. Only after that, measurements in the investigated range were carried out.

Indeed, the anomalies at 180 and 240 K became 4 times smaller in magnitude but did not disappear. Another evidence that the anomalies at 180 and 240 K in these crystals are not due to the domain structure (although certainly related), in Fig. 6(b) shows the thermoluminescence curve of $Sn_2P_2S_6$ crystals. And although thermoluminescence is very sensitive to the defectivity of the structure,[25] which could be the domain walls, this phenomenon is present in the range of 100–300 K not in all $Sn_2P_2S_6$ crystals,[13] and domains are in all. In addition, the presence of photoluminescence in the low-temperature region[14] and the above-mentioned anomalies of dielectric permittivity at 60 K[12] also testify to the different nature of these anomalies.

"Domain contribution" to dielectric losses can be easily explained by the effects of hysteresis anomalies at 190 and 280 K for crystals obtained by the Bridgman method [Figs. 1(b) and 1(d)] and the absence of hysteresis in gas-transport crystals [Figs. 2(b) and 2(d)]. As mentioned at the beginning of this section, freezing (or "pinning") of the domain structure is observed in the 160–280 K region, which is strongly related to the conductivity of the samples. In crystals with high conductivity, charged domain walls are anchored on charged structural defects, which significantly reduces their mobility. Accordingly, the hysteresis is weak (practically absent), as we can see in Figs. 2(b) and 2(d). In the case of high resistivity crystals, the concentration of charged defects is much less, because of which the domain walls are fixed weaker, which is manifested as a strong hysteresis of anomalies at 190 and 280 K for crystals obtained by the Bridgman method [Figs. 1(b) and 1(d)].

From the above, we can conclude that although the domain structure is not the exclusive cause of dielectric permittivity and loss anomalies in the low-temperature region of $Sn_2P_2S_6$ crystals, it has a significant influence on them.

4.6. Relaxation processes

As it was noted by all authors who investigated low-temperature anomalies of dielectric permittivity,[12,17] they exhibit relaxation character. Therefore, we measured the frequency dependence of dielectric permittivity in the frequency range 12 Hz–100 kHz and the temperature range 100–280 K for crystals obtained from the gas phase (as a reference). The anomalies at temperatures 200 and 260 K shift towards higher temperatures with increasing frequency, which indeed indicates their relaxation nature.

Temperature-frequency variations of the obtained dielectric data are well described by the Arrhenius relation $\upsilon = \upsilon_0 \exp(E_A/kT)$, where E_A is the activation energy. For the gas-transport crystals we studied, $E_A \approx 0.27$ eV for the low-temperature and 0.5 eV for the high-temperature anomaly. Our previously published work[17] carried out similar studies for crystals obtained by the Bridgman method and obtained similar values of $E_A \approx 0.23$ and 0.57 eV, respectively, which as indicated in the introduction is quite explained by the variation in the parameters of $Sn_2P_2S_6$ crystals obtained by different methods.

We also plotted Cole-Cole diagrams (Fig. 7) at different temperatures, which can be described by an empirical formula:

$$\varepsilon^* = \varepsilon_\infty + \frac{\Delta\varepsilon}{1 + (i\omega\tau)^{1-\alpha}},$$
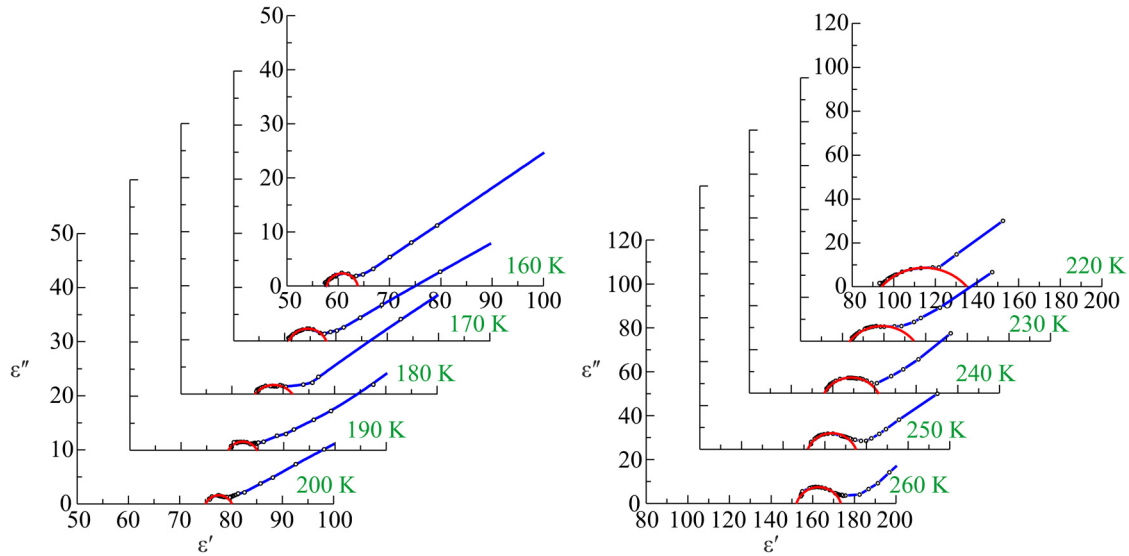
12 January 2024 09:20:23

FIG. 7. Cole-Cole diagrams at different temperatures for gas transport $Sn_2P_2S_6$ crystal.

where $\Delta\varepsilon$ is the dielectric relaxation strength, τ is the average or most probable Cole-Cole relaxation time, ε_∞ is the contribution of all polar phonons and electron polarization to the dielectric permittivity, $0 \le \alpha \le 1$ is the blurring factor or the width parameter of the Cole-Cole distribution functions. At $\alpha = 0$, this equation reduces to Debye's formula. From the experimental data obtained (Fig. 7), it was found that the smearing parameter is $\alpha \approx 0.5$ for both the low-temperature (160–200 K) and high-temperature (220–260 K) anomaly.

5. THEORETICAL CONSIDERATIONS

In Ref. 24 it was clearly shown that the semiconducting properties of $Sn_2P_2S_6$ crystals are due to deep donor levels of ≈ 0.4 eV in the gap, which are caused by sulfur vacancies and relatively shallow acceptor levels of ≈ 0.1 eV associated with tin vacancies. In addition, in the forbidden zone of these crystals, there are deep energy levels due to electron polarons of a small radius and relatively shallow energy levels of hole polarons of a small radius. Electron polarons are captured by traps of Sn^+ cations, and hole polarons are in traps of S^- anions. Based on the obtained theoretical calculations, an energy scheme of $Sn_2P_2S_6$ crystals[24] was constructed and is presented in Fig. 8. This scheme allowed us to successfully explain both photoluminescence[14] and thermoluminescence[13] spectra, photoinduced EPR signals,[26] and photorefractive and thermoelectric properties of $Sn_2P_2S_6$ crystals.[27]

The low-temperature relaxation dielectric anomalies discussed in the experimental part of our work can also be easily interpreted using the energy scheme from Fig. 8 and the motion of polarons in the external measurement field.[17] The polaron mechanism of the observed anomalies is evidenced by the coincidence of the experimentally obtained relaxation energies at 160 K (≈ 0.27 eV) and at

260 K (≈ 0.5 eV) with the values that can be obtained on the basis of the proposed energy scheme. Dielectric losses of the first of them (160–200 K) are most likely caused by the reorientation of hole polarons, which are associated with a smaller non-equilibrium of chemical bonds and a larger amplitude of thermal motions of ions with activation energy $E_A = 0.3$ eV. And higher temperature anomaly of dielectric losses (200–280 K) can be related to the translational motion of hole polarons, which are supported by donor-acceptor compensation with activation energy $E_A = 0.5$ eV.
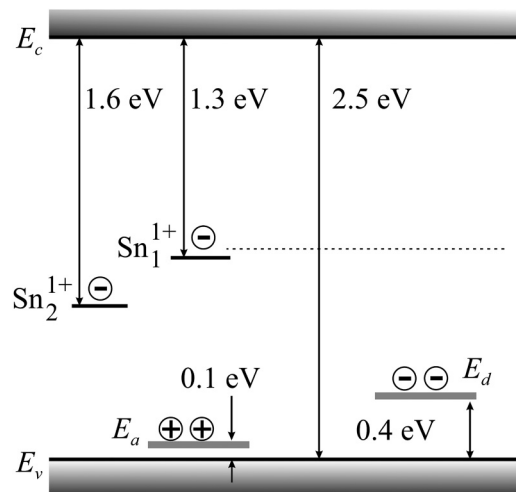

FIG. 8. Energy diagram of $Sn_2P_2S_6$ crystals with vacancies of tin and sulfur for acceptor (E_a), donor (E_d), and small electronic polarons (Sn_1^{1+}, Sn_2^{1+}) energy levels.[17]

The increase in the concentration of sulfur vacancies, in the case of $Sn_{2.05}P_2S_{5.95}$, increases the concentration of charge carriers at the deep donor levels ≈ 0.4 eV, and the increase in the concentration of tin vacancies in the case of $Sn_{1.95}P_2S_{6.05}$ crystals increase the concentration of charge carriers at the shallow acceptor levels ≈ 0.1 eV, and in both cases leads mainly to an increase in the dielectric loss anomaly in the lower temperature region (160–200 K), while the anomaly in the 200–280 K region decreases strongly (for $Sn_{1.95}P_2S_{6.05}$) or disappears altogether (for $Sn_{2.05}P_2S_{5.95}$).

Such behavior can be explained by a strong increase in the concentration of polarons, which will appear as an increase in the low-temperature dielectric loss anomaly, and a strong imbalance in the concentration of charge carriers at the donor and acceptor levels for samples obtained with a significant deviation in stoichiometry, that will reduce the donor-acceptor compensation. It will reduce the translational mobility of hole polarons, which leads to a decrease (or disappearance) of $\varepsilon''(T)$ at 200–280 K.

A strong increase in the concentration of donor or acceptor carriers in the case of crystals grown with stoichiometry deviation leads to an overall increase in dielectric losses (even compared to the crystal obtained by the CTR method), as can be seen in Figs. 3(b) and 3(d), while polarization shielding decreases the dielectric constant [Fig. 3(a)].

6. CONCLUSIONS

The low-frequency dielectric susceptibility relaxation anomalies in $Sn_2P_2S_6$ crystals in the 100–280 K region could be related to the small hole polarons dynamics with donor-acceptor compensation processes in lattice with tin and sulfur vacancies.[17] To prove this, we investigated $Sn_2P_2S_6$ crystals grown with stoichiometry deviation, with increased sulfur content $Sn_{1.95}P_2S_{6.05}$ and increased tin content $Sn_{2.05}P_2S_{5.95}$. As could be expected, such a change in chemical composition significantly affected the shape and amplitude of low-temperature anomalies of dielectric permittivity and losses. The increase in the concentration of sulfur vacancies, in the case of $Sn_{2.05}P_2S_{5.95}$, increases the concentration of charge carriers at the deep donor levels ≈ 0.4 eV, and the increase in the concentration of tin vacancies in the case of $Sn_{1.95}P_2S_{6.05}$ crystals increase the concentration of charge carriers at the shallow acceptor levels ≈ 0.1 eV, and in both cases leads mainly to an increase in the dielectric loss anomaly in the temperature region (160–200 K), while the anomaly in the 200–280 K region decreases strongly (for $Sn_{1.95}P_2S_{6.05}$) or disappears altogether (for $Sn_{2.05}P_2S_{5.95}$).

REFERENCES

[1]Yu. M. Vysochanskii, T. Janssen, R. Currat, R. Folk, J. Banys, J. Grigas, and V. Samulionis, *Phase Transitions in Ferroelectric Phosphorous Chalcogenide Crystals* (Vilnius University Publishing House, 2006).
[2]I. Zamaraite, S. Svirskas, Y. Vysochanskii, K. Glemza, J. Banys, and A. Dziaugys, Phase Transitions **92**, 500 (2019).
[3]M. M. Maior, I. P. Prits, V. T. Vrabel, Yu. M. Vysochanskii, M. V. Potorii, A. A. Kikineshi, M. Kis-Varga, and A. Csik, Ferroelectrics Lett. Sec. **33**, 31 (2006).
[4]I. Zamaraite, R. Yevych, A. Dziaugys, A. Molnar, J. Banys, and S. Svirskas, and Yu. Vysochanskii, Phys. Rev. Appl. **10**, 034017 (2018).
[5]A. Molnar, D. Gal, H. Ban, and V. Gerasimov, Integrated Ferroelectrics **220**, 110 (2021).
[6]A. A. Grabar, I. V. Kedyk, M. I. Gurzan, I. M. Stoika, and A. A. Molnar, and Yu. M. Vysochanskii, Optics Communications **188**, 187 (2001).
[7]M. M. Maior, M. I. Gurzan, S. B. Molnar, I. P. Prits, and Yu. M. Vysochanskii, Trans. of Ultrasonics. Ferroelectrics and Frequency Control **47**, 877 (2000).
[8]I. P. Pritc, Yu. V. Voroshilov, and M. V, Potoriy, Inorganic Materials **26**, 2363 (1990).
[9]R. Nitsche and P. Wild, Materials Research Bulletin **5**, 419 (1970).
[10]A. A. Molnar, Yu. M. Vysochanskii, A. A. Horvat, and Yu. S. Nakonechnii, Ferroelectrics **174**, 41 (1995).
[11]A. A. Horvat, A. A. Molnar, Yu. M. Vysochanskii, and Yu. S. Nakonechnii, "Uzhhorod university scientific herald," Series Physics **1**, 50 (1997).
[12]M. Iwata, A. Miyashita, Y. Ishibashi, K. Moriya, and S. Yano, J. Phys. Soc. Jpn. **67**, 499 (1998).
[13]Z. Potucek, P. Ptacek, and Z. Bryknar, Phys. Status Solidi C **2**, 560 (2005).
[14]Z. Potucek and Z. Bryknar, Ferroelectrics **334**, 171 (2006).
[15]Z. Potucek, Z. Bryknar, and P. Ptacek, Ferroelectrics **304**, 181 (2004).
[16]M. M. Medulich, M. M. Major, A. A. Kogutich, and S. F. Motrya, "Uzhhorod university scientific herald," Series Physics **34**, 22 (2013).
[17]Yu. Vysochanskii, A. Molnar, R. Yevych, K. Glukhov, and M. Medulych, Ferroelectrics **440**, 31 (2012).
[18]A. I. Pogodin, T. O. Malakhovska-Rosokha, O. P. Kohan, and D. V. Sevryukov, "Uzhhorod university scientific herald," Series Chemistry **2**, 21 (2012).
[19]H. Bán, D. Gal, V. Gerasimov, A. Haysak, and A. Molnar, *IDAACS 2021 the 11th IEEE International Conference on Intelligent Data Acquisition and Advanced Computing Systems: Technology and Applications, September 22–25* (Cracow, Poland, 2021), p. 156.
[20]A. A. Molnar, "Uzhhorod university scientific herald," Series Physics **40**, 148 (2016).
[21]C. B. Sawyer and C. H. Tower, Phys. Rev. **35**, 269 (1932).
[22]V. Shvalya, J. Zavašnik, V. Nasretdinova, H. Uršič, J. Kovač, A. Grabar, A. Kohutych, A. Molnar, D. R. Evans, D. D. Mihailović, and U. Cvelbar, J. Mater. Chem. C **8**, 9975 (2020).
[23]S. Huang, C. Meng, M. Xiao, S. Ren, S. Wang, D. Han, and Y. Li, and Yu. Meng, Small **14**, 1704367 (2018).
[24]Yu. Vysochanskii, K. Glukhov, M. Maior, K. Fedyo, A. Kohutych, V. Betsa, I. Prits, and M. Gurzan, Ferroelectrics **418**, 124 (2011).
[25]A. J. J. Bos, Materials **10**, 1357 (2017).
[26]A. Rudiger, O. Schirmer, S. Odoulov, A. Shumelyuk, and A. Grabar, Optical Materials **18**, 123 (2001).
[27]T. Babuka, K. Glukhov, A. Kohutych, Yu. Vysochanskii, and M. Makowska-Janusik, Cryst. Eng. Comm. **22**, 2336 (2020).

12 January 2024 09:20:23